BIOCHEMISTRY
including biophysical chemistry & molecular biology

Article

pubs.acs.org/biochemistry

Critical Role of Asp227 in the Photocycle of Proteorhodopsin

Julia Herz,[‡] Mirka-Kristin Verhoefen,[‡] Ingrid Weber,[§] Christian Bamann,[∥] Clemens Glaubitz,[§] and Josef Wachtveitl*,[‡]

[‡]Institute of Physical and Theoretical Chemistry, Johann Wolfgang Goethe-University, Max von Laue-Straße 7, 60438 Frankfurt am Main, Germany

[§]Institute of Biophysical Chemistry and Center of Biomolecular Magnetic Resonance, Johann Wolfgang Goethe-University, Max von Laue-Straße 9, 60438 Frankfurt am Main, Germany

[∥]Max Planck Institute of Biophysics, Max von Laue-Straße 3, 60438 Frankfurt am Main, Germany

ABSTRACT: The photocycle of the proton acceptor complex mutant D227N of the bacterial retinal protein proteorhodopsin is investigated employing steady state pH-titration experiments in the UV−visible range as well as femtosecond-pump−probe spectroscopy and flash photolysis in the visible spectral range. The evaluation of the pH-dependent spectra showed that the neutralization of the charge at position 227 has a remarkable influence on the ground state properties of the protein. Both the pK_a values of the primary proton acceptor and of the Schiff base are considerably decreased. Femtosecond-time-resolved measurements demonstrate that the general S_1 deactivation pathway; that is, the K-state formation is preserved in the D227N mutant. However, the pH-dependence of the reaction rate is lost by the substitution of Asp227 with an asparagine. Also no significant kinetic differences are observed upon deuteration. This is explained by the lack of a strongly hydrogen-bonded water in the vicinity of Asp97, Asp227, and the Schiff base or a change in the hydrogen bonding of it (Ikeda et al. (2007) *Biochemistry 46*, 5365−5373). The flash photolysis measurements prove a considerably elongated photocycle with pronounced pH-dependence. Interestingly, at pH 9 the M-state is visible until the end of the reaction cycle, leading to the conclusion that the mutation does not only lower the pK_a of the Schiff base in the unphotolyzed ground state but also prevents an efficient reprotonation reaction.

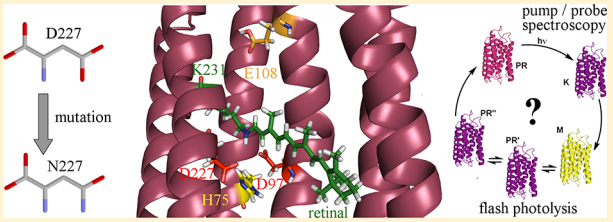

Retinal proteins are widely spread in nature. They exist in all three domains of living organisms and function as visual pigments, light-activated ion pumps or channels, and phototactic sensors.[1−8] All of these proteins share common structural motifs even if they have different origins. They are membrane proteins composed of seven transmembrane helices forming the binding pocket in which a retinal chromophore is covalently bound to the ε-amino group of a conserved lysine in the helix G via a Schiff base linkage.

A sequence comparison of the bacterial proton pump proteorhodopsin (PR) and the archaeal bacteriorhodopsin (BR) revealed considerable homology for the residues forming the binding pocket.[9] With the exception of the release complex, all residues involved in proton transport across the membrane are conserved. Together with the knowledge of the recently resolved NMR structure,[10] it is not surprising that PR exhibits a photochemical reaction cycle with intermediates and kinetics similar to the archaeal BR.

For PR, upon light excitation the ultrafast isomerization of the retinal from the all-*trans* to the 13-*cis* conformation is induced, which triggers a sequence of protein conformational changes including several proton transfer reactions.[11−13] On the basis of the models for BR,[4,14−16] Lenz et al. proposed a branched reaction scheme for the primary reaction dynamics of PR.[17] The C=C stretching is supposed to be the first reaction coordinate out of the Franck−Condon region before the torsion around the C_{13}−C_{14} bond takes place leading to a conical intersection (CI) with the ground state. The observed biexponential deactivation of the excited state was explained by the assumption that some molecules do not directly reach the CI and end up in a local minimum on the S_1 potential energy surface (PES), which has to be overcome first. Particularly, it could be shown that the deactivation of the excited state possesses a pronounced pH-dependence explained by a pH-dependent tilting of the S_1 potential energy surface.[17] However, femtosecond infrared spectroscopy showed that the quantum efficiency of the primary photointermediate, the K-state, is not affected by the pH/pD value.[18]

In addition to the primary photodynamics, the subsequent, thermally driven photocycle steps are also pH-sensitive. Under alkaline conditions several studies demonstrated the appearance of four additional intermediates which were termed PR_L, PR_M, PR_N, and PR_O.[12,13,19−21] The transition rates vary depending on the sample conditions (solubilization or reconstitution, buffer, pH-value).[22] Consistently it was reported that not pure intermediates are observed but equilibria of several species. The photocycle under acidic conditions is characterized by

Received: March 23, 2012
Revised: June 27, 2012
Published: June 27, 2012

   dx.doi.org/10.1021/bi3003764 | *Biochemistry* 2012, 51, 5589−5600

three red-shifted intermediates (PR_L, PR_N, and PR_O), but no evidence for the appearance of the blue-shifted M-state could be found at room temperature.[13,21,23] However, in low temperature measurements an M-like intermediate could be verified at acidic pH.[24] Along with the photocycle characteristics, the proton pumping direction changes with pH. At pH-values >8 PR exhibits a BR-like outward directed proton transport. The direction of the proton transport is inverted at acidic pH-values.[13,24]

The variable vectoriality of the proton flow is supposed to be connected to the protonation state of the primary proton acceptor Asp97. Interestingly, the pK_a of Asp97 (pK_a = 7.0−8.2) in PR[12,13,25] is much higher than that of the homologous Asp85 in BR (pK_a = 2−3).[15,16] The presence of a highly conserved histidine residue at position 75 which interacts directly with Asp97 was recently described as a major determinant for this finding.[26,27]

Although Asp97 is proposed to be the primary counterion of the protonated Schiff base, Ikeda et al. suggested that also Asp227 plays a crucial role in the photocycle of PR, especially during the photoisomerization.[28] The latter point was further verified by ultrafast IR measurements.[29] By means of FTIR spectroscopy a strong interaction between the protonated Schiff base and the negatively charged Asp227 (pK_a = 2.6[30]) by a strongly hydrogen bonded water molecule was shown. Replacement of Asp227 by an asparagine results in an altered environment in the binding pocket due to the loss of the negative charge. Consequently the D227N mutant lacks this hydrogen bond.[28] Further studies of the D227N mutant showed that Asp227 is also responsible for the selectivity of retinal photoisomerization. The observation of an increased concentration of the 9-*cis* photoproduct in the D227N mutant indicates that the Asp227 anion facilitates the all-*trans* to 13-*cis* photoisomerization and restricts formation of other conformers.[30]

For the purpose of getting deeper insights into the primary reaction steps of PR, we studied the D227N mutant at pH 4.0 (protonated Asp97) and pH 9.0 (deprotonated Asp97) using femtosecond-vis-pump/vis-probe spectroscopy. The present study includes measurements in H_2O and D_2O in order to investigate the influence of previously proposed water clusters in the binding pocket. Moreover, the subsequent photocycle steps are addressed by means of pH-dependent flash photolysis measurements.

MATERIALS AND METHODS

Preparation of PR Samples. The PR gene was cloned in the pET-27b(+) vector (Novagene, Merck, Darmstadt, Germany). We regard this protein as the wt and introduced the single point mutation D227N. For preparation of the expression plasmids of the mutant, a QuikChange site-directed mutagenesis kit (Stratagene, Agilent Technologies, Waldbronn, Germany) was used according to the standard protocol. The correct mutation has been verified by sequence analysis of the complete gene. Expression and purification of both the wt and the D227N sample were carried out as described earlier by Hempelmann et al.[27]

Retinal Extraction Experiments. In order to estimate the ratio of different retinal isomers in the ground state the isomer composition of the PR D227N mutant at pH 4 and pH 9 was determined by extraction experiments as described by Scherrer et al.[31] In analogy to BR we assume the isomeric composition not to be dependent on the isotope of the solvent.[32] Extraction experiments were therefore only performed in H_2O. We ascribe the higher signal intensity of the deuterated PR D227N samples in the UV (Figure 1) to the buffer exchange procedure which in terms causes higher scattering of the samples and/or a higher UV absorption due to the absorption of degradation products. A possible change in the retinal beta-band with an increase in absorption for 13-*cis* retinal compared to the all-*trans* isomer could also be imagined. However, the changes in the UV for the different isomers are at least for BR not very pronounced,[33] which is why we consider this case to be improbable.

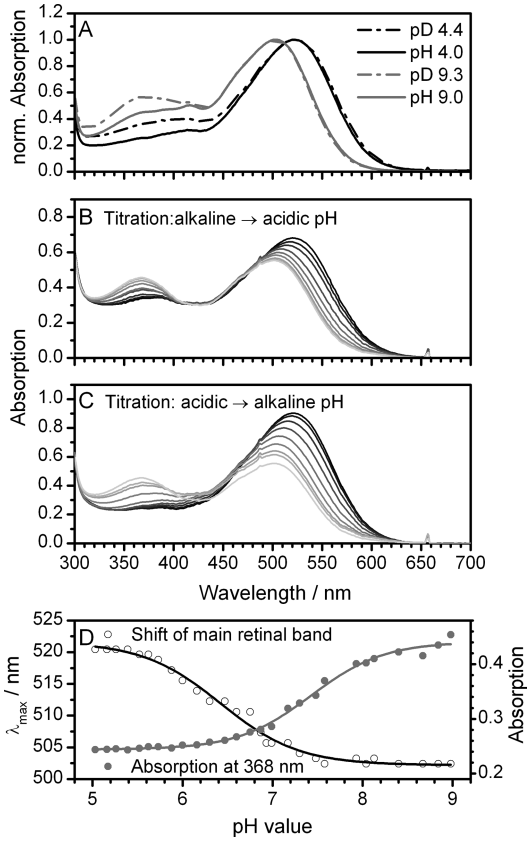

Figure 1. A comparison of the PR D227N absorption spectra recorded in H_2O (solid line) and D_2O (dash-dotted line) at pH/pD 4 (black) and pH/pD 9 (gray) is depicted in (A). (B) and (C) show the UV−vis absorption spectra recorded between pH 9 (gray) to pH 5 (black) in steps of ~0.5 pH units for both titration directions. For analysis either the wavelength of the shifting absorption maximum or the absorption at 368 nm was plotted against the pH-value (shown for the acidic → alkaline pH-titration in D). A Boltzmann fit of this plot provides the pK_a value of the deprotonation/protonation reaction of Asp97 (λ_{max} vs pH) or the Schiff base (absorption at 368 nm vs pH).

The D227N samples were dark adapted for 16 h at room temperature. The extraction and all subsequent steps were done under dim-red light conditions. The chromophore samples were dissolved in the mobile phase consisting of a hexane/ethylacetate mixture of 90:10 [v:v] and injected into a normal phase HPLC (Merck LaChrome D-7000 system, Darmstadt, Germany) and separated on a ProntoSIL-OH 120-3 column (Bischoff GmbH, Leonberg, Germany). The HPLC peaks have been assigned to the different isomers using commercially available standards. For 13-*cis*, 9-*cis*, and all-*trans* retinal retention times of 4.06, 4.25, and 4.64 min, respectively, have been found. Since the retention times of the retinal isomers

dx.doi.org/10.1021/bi3003764 | Biochemistry 2012, 51, 5589−5600

extracted from the samples nicely coincide with those of the standards it is assumed that only these conformers are present in the D227N samples.

For analysis the area of the HPLC peak was determined in a first step. This value was taken as the optical density at the HPLC probing wavelength of 360 nm. On the basis of the Lambert−Beer Law the relative concentrations of the isomers were calculated using the different molar extinction coefficients of the isomers.[34]

pH-Titration. For the pH-titration the PR sample was dissolved in a buffer that consists of 50 mM sodium citrate, 50 mM sodium phosphate, 50 mM tris(hydroxymethyl)-aminomethane (TRIS), 50 mM boric acid, 100 mM sodium chloride, and 0.1% *n*-dodecyl-*β*-D-maltoside (DDM). pH-dependent UV−vis spectra of the sample were taken using an Analytik Jena spectrometer (S 100 spectrometer, Analytik Jena, Jena, Germany). The titration was carried out in a 1 × 1 cm cuvette, where the sample had an absorption of 0.5−1. To guarantee an optimal mixing of the sample it was continuously stirred. The pH value was measured with a calibrated pH-meter (pH 320 SET microprocessor pH-meter, WTW GmbH, Weilheim, Germany; Biotrode pH electrode, Hamilton Messtechnik GmbH, Höchst, Germany). To ensure the reversibility of the reaction the titration was performed in both directions (alkaline → acidic pH; acidic → alkaline pH). The starting pH-values of 9.0 or 5.0, respectively, were adjusted by adding NaOH or HCl solutions to the buffer. The HCl and NaOH solutions were highly concentrated to avoid concentration changes of the sample due to increasing volumes. During the titration HCl or NaOH was added and UV−vis spectra were recorded approximately every 0.2 pH-units.

For analysis, either the wavelength of the absorption maximum of a shifting band or the absorption of a certain wavelength was plotted against the pH. The resulting sigmoidal curve was fitted with a Boltzmann function:

$$y = A_2 + \frac{(A_1 - A_2)}{1 + \exp\left(\frac{(x - x_0)}{dx}\right)} \quad (1)$$

The inflection point x_0 was directly taken as the pK_a value of the observed protonation reaction. The stated errors are estimated and consist among other things of calibration inaccuracies of the pH-meter and fitting errors.

Vis-Pump/vis-Probe Spectroscopy. The femtosecond-time-resolved measurements of the PR D227N mutant were performed either in 50 mM citrate buffer with 100 mM NaCl and 0.1% DDM at pH 4.0/pD 4.4 or in 50 mM TRIS buffer with 100 mM NaCl and 0.1% DDM at pH 9.0/pD 9.3. The exchange of the buffer solutions and the adjustment of the concentration were achieved by Centricon centrifugal filters (10 kDa MW cutoff; Vivascience, Sartorius Group, Hannover, Germany). The concentration was adjusted to an optical density of about 0.5 in a fused silica cuvette with an optical pathway of 1 mm.

The pump−probe experiment is constructed as described in Lenz et al.[17] A femtosecond-laser system (CLARK CPA 2001, Clark-MXR, Dexter, MI, USA) served as the pulse source for the experiment. To generate the excitation pulses at wavelengths of 505 and 520 nm, respectively, a noncollinear optical parametric amplifier (NOPA) was applied.[35] The excitation pulses had pulse energies of approximately 50 nJ and a focal diameter of about 150 μm. The super continuum white light probe pulses were generated by focusing the laser fundamental in a sapphire plate (2.3 mm thickness). The resulting white light pulses were polarized parallel with respect to the excitation pulses. Anisotropy effects due to rotational diffusion are slow for large proteins,[36] which is why polarization of pump and probe pulse in the magic angle is not important. A spectral range of 440−750 nm was covered in the experiments with a resolution of approximately 8 nm and a sensitivity of 10^{-4} absorbance change units. The cross-correlation width (temporal resolution) gradually changed from 60 to 80 fs as the probe pulses moved from short to long wavelengths. To guarantee the exchange of the sample volume for successive laser pulses, the sample was moved laterally. UV−vis spectra were recorded before and after the pump/probe experiment to ensure that no photodegraded proteins were accumulated.

Global Fit Analysis. Initially, the transient absorption data were corrected for coherent effects around delay time zero by subtracting the buffer signal measured under identical conditions.[37] The data were adjusted for group velocity dispersion by observing the temporal and spectral evolution of the coherent signal of the pure buffer solution. For the quantitative analysis, a kinetic model was used, which describes the data as a sum of exponential decays. A Marquardt downhill algorithm optimizes n global time constants τ_i simultaneously with wavelength-dependent amplitudes $A_i(\lambda)$ for each component τ_i. Gaussian pump and probe pulses with a (1/e)-cross correlation width t_{cc} are assumed:

$$\Delta A(t, \lambda) = \sum_{i=1}^{n} A_i(\lambda) \exp\left(\frac{t_{cc}^2}{4\tau_i^2} - \frac{t}{\tau_i}\right)\frac{1}{2} \left(1 + \mathrm{erf}\left(\frac{t}{t_{cc}} - \frac{t_{cc}}{2\tau_i}\right)\right) \quad (2)$$

Positive amplitudes are indicative for the decay of positive absorbance changes and the formation of negative ones, whereas negative amplitudes reflect the decay of negative absorbance changes and the growth of positive contributions. An infinite time constant is equal to a time-independent offset (for $t \gg t_{cc}$) and can be interpreted as the signal, which remains at the maximum delay time of the experiment (1.5 ns). The errors of the time constants given in Tables 2 and 3 are estimated by a comparison of global fit analyses using different sets of parameters (number of decay time constants, starting values, time zero, time window).

Fourier Analysis. For the characterization of the coherent effects appearing around delay time zero a global fit that only describes the decay components >250 fs was subtracted from the transients. The resulting residuals contain only the fast oscillating signal. For the evaluation all data points ≥2 ps were discarded, leading to a data set with an x-axis spanning between approximately −1.9 to 2 ps. The time points were interpolated and in the same process set to 1/4 of the original distance (33 to 8.2 fs). The absorbance change values at delay times which do not show the fast coherent signals were defined to be zero. This procedure is similar to the so-called "zero filling" or "zero padding" and should not cause artifacts or falsification. For a quantitative analysis, the processed residuals were evaluated by fast Fourier transformation (FFT)[38,39] using the Blackman window method. As the outcome the resulting power spectra are presented. Because of the time resolution of approximately 60 fs, frequencies can be resolved up to 560 cm^{-1}.

Flash Photolysis. A detailed description of the laser flash photolysis setup can be found in Verhoefen et al.[40] For the

dx.doi.org/10.1021/bi3003764 | *Biochemistry* 2012, 51, 5589−5600

performed measurements excitation pulses with a central wavelength of 502 and 505 nm were provided by a laser-pumped optical parametric oscillator system (Spitlight 600, Innolas Laser GmbH, Krailing, Germany; GWU Lasertechnik, Erftstadt, Germany). The pulses had a duration of approximately 20 ns and an energy of 2 mJ cm^{-2}. The laser was operated at a repetition rate of 0.25 Hz combined with an external shutter blocking two of three pulses. This led to an interval of 12 s between two subsequent excitation pulses. A halogen lamp (LC8, Hamamatsu, Herrsching, Germany) served as probe source. The probe light was spectrally filtered using a monochromator (Photon Technology International, Birmingham, NJ, USA) and focused into the sample cell (fused silica cuvette, 1 × 1 cm) with an angle of 90° with respect to the direction of the excitation beam. The probe light intensities were low enough to avoid actinic effects. After passing through the cuvette the probe beam was focused onto the entrance slit of a second monochromator. The signal was detected by a photomultiplier (Photosensor H6780-02, Hamamatsu, Herrsching, Germany) and recorded with a digital storage oscilloscope (Waverunner 62xi, LeCroy, Geneva, Switzerland). For each scan, data points were collected between −200 ms and 9.8 s with a time base of 1 μs; 1000 scans were averaged. In order to reduce the data set, the linear time base was converted to an exponential one for 15 $\mu s < t < 9.8$ s (300 points) by averaging the absorbance changes for the time interval between the exponentially increasing points. The flash photolysis data were analyzed using the global fitting procedure described for the vis-pump/vis-probe data.

RESULTS

Retinal Extraction Experiments. The isomeric composition of the used PR D227N samples was determined as described in Scherrer et al.[31]

The peaks were assigned to the isomers using the HPLC traces of the isolated retinal standards recorded under identical conditions. The good agreement of the retention times of 13-*cis*, 9-*cis*, and all-*trans* retinal with the peaks of the isolated species of the PR D227N samples leads to the conclusion that only these retinal isomers are present in the mutant at pH 4.0 and pH 9.0.

Table 1 summarizes the individual results of the D227N samples under alkaline and acidic conditions. At pH 4.0 roughly

Table 1. Retinal Isomer Ratios of the D227N Mutant Determined in Extraction Experiments[a]

sample	% all-*trans*	% 13-*cis*	% 9-*cis*
D227N, pH 9.0	67	32	1
D227N, pH 4.0	76	22	2

[a]The error of each value is estimated to be in the range of 2%.

22% 13-*cis* and 76% all-*trans* retinal are present in the ground state. The 13-*cis* contents of the sample increases under alkaline conditions. At pH 9.0 32% 13-*cis* and 67% all-*trans* retinal have been calculated. The fraction of the 9-*cis* retinal is ≤2% at both pH-values.

pH-Titration. Figure 1A−C shows the absorption spectra for the PR D227N mutant with respect to the pH-value. During the titration the pH was either varied from alkaline to acidic pH-values (Figure 1B) or from acidic to alkaline pH-values (Figure 1C). Both series of curves exhibit the same general features: The main absorption band shows a red-shift of about 20 nm with decreasing pH (λ_{max}(pH 9) = 502 nm, λ_{max}(pH 5) = 522 nm). This shift is already known from PR wt[13] and has been attributed to the protonation change of the primary proton acceptor Asp97. Figures 1B and C demonstrate that the extinction coefficient of the main absorption band drops with increasing pH. Concomitantly, a further band appears around 370 nm. Like for the main retinal band a bathochromic shift is observed when lowering the pH (λ_{max}(pH 9) = 368 nm, λ_{max}(pH 5) = 389 nm). The band vanishes almost completely when the pH is decreased to acidic pH-values again, verifying that its main origin is not a degradation product or unbound retinal. The band position alludes to a deprotonated Schiff base configuration of the chromophore. Second, an assignment to the beta-band of a 13-*cis* retinal which exhibits a higher absorption compared to the all-*trans* isomer cannot be fully excluded. However, the changes in the near-UV for the different isomers are at least for BR not very pronounced,[33] favoring the first interpretation.

For the determination of the pK_a value of the primary proton acceptor, the absorption maximum of the main retinal band was plotted against the pH-value, and the resulting curve was fitted using a Boltzmann function (see Figure 1D). The inflection point of the curve is interpreted as pK_a of Asp97. The titration direction solely affects the pK_a, indicative for a reversible protonation/deprotonation reaction. The pK_a was determined to be 6.1 ± 0.2 in the alkaline→ acidic and 6.4 ± 0.2 in the acidic → alkaline pH-titration.

As stated above, the absorption maximum of the band centered around 370 nm suggests the assignment to a retinal with a deprotonated Schiff base. The acidic → alkaline pH-titration shows the incipient formation of this band at neutral pH. However, the reaction seems not to be fully reversible since a remaining small contribution is observed at the end of the alkaline → acidic pH-titration. In order to analyze this characteristic transition, the absorption at 368 nm was plotted against the pH-value (Figure 1D). The typical sigmoid shape of this curve suggests that the main part of the observed transition is based on a protonation/deprotonation reaction, in this case most likely the deprotonation of the Schiff base. The inflection point of the plot is interpreted as pK_a of the Schiff base. For PR D227N it is found at 7.4 ± 0.2 for the acidic → alkaline pH-titration. In case of the alkaline → acidic pH-titration the pH-induced decrease of the absorption at 368 nm is less articulated and the transition is not as sharp, resulting in an imprecise quantitative evaluation.

UV−vis Absorption Spectra in H_2O and D_2O. Figure 1A contrasts the UV−vis spectra of the D227N mutant in H_2O and D_2O. The absorption maximum of the main retinal band is not shifted in the deuterated samples and remains at 522 nm for pH/pD 4 and at 502 nm for pH/pD 9. However, both D_2O-samples show a constant offset between 300 and 450 nm, originating from an increased scattering background, and do not exhibit a distinct maximum at 370 nm.

vis-Pump/vis-Probe Experiments. Femtosecond-transient absorption measurements of the PR D227N mutant were carried out in H_2O and D_2O at two distinct excitation wavelengths depending on the protonation state of the primary proton acceptor. Experiments were performed either at pH 4.0/pD 4.4 (below the pK_a of Asp97) with an excitation wavelength of 520 nm or at pH 9.0/pD 9.3 (above the pK_a of Asp97) using an excitation wavelength of 505 nm. Figure 2 gives an overview about the resulting pD-dependent absorbance changes of PR D227N. A closer look at the characteristics of the transient

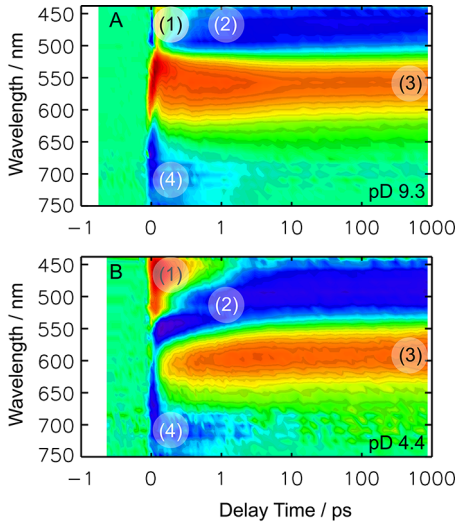

Figure 2. Transient absorbance changes of PR D227N at pD 9.3 (A) and 4.4 (B) after photoexcitation at 505 and 520 nm, respectively. The amplitudes are color coded: red, positive; green, zero; blue, negative absorbance changes. The time axis is linear in the range from −1 ps to +1 ps and logarithmic for longer delay times. The spectra are dominated by the excited state absorption (1), ground state bleaching (2), the absorption of the photoproduct (3), and stimulated emission (4).

absorbance changes of each pD/pH pair provides evidence that the dynamics are independent of the H/D exchange within the accuracy of the experiment (see Figure 3A–D). The apparent small differences between the transients of pH 4.0 and pD 4.4 (see Figure 3B,D) could result from anisotropy effects of the pump and the probe beam. The relative orientation between the beams has an inaccurancy of approximately 5°. Further on, small differences in the experimental settings, such as the calibration of the white light could also explain the slightly different decay of the transients at pD 4.4. Because the better signal-to-noise ratio, the results are discussed for the deuterated samples.

In general, at both protonation states of Asp97 four characteristic spectral features show up in the measured difference spectra. At pH/pD 9 a very short-lived negative signal between 440 and 500 nm precedes to a positive absorbance change within the cross correlation time (Figure 3A). This positive contribution (region (1) in Figure 2A) decays on a 100 fs time scale. It can be assigned to the absorption of the excited state. The positive signature is followed by a negative one (region (2) in Figure 2A) at delay times > 0.5 ps. This negative contribution is assigned to the depopulated ground state. Around 500–600 nm positive absorbance changes are observed for the whole investigated time range (Figure 3C). At delay times < 200 fs a very fast (20 fs) decay of the initial signal is observed. Afterward it rises again until 500 fs and then decays slightly with a time constant around 5 ps. The signal at long delay times can be unambiguously assigned to the absorption of the K-like photoproduct (region (3) in Figure 2A), with its isomerized 13-*cis* retinal chromophore. At early delay times fractions of the excited state absorption also contribute to the observed signature. In the red part of the investigated spectral region the negative difference signature of the stimulated emission is observed (region (4) in Figure 2A). Figure 3E illustrates that the signal decays nearly completely within 7 ps.

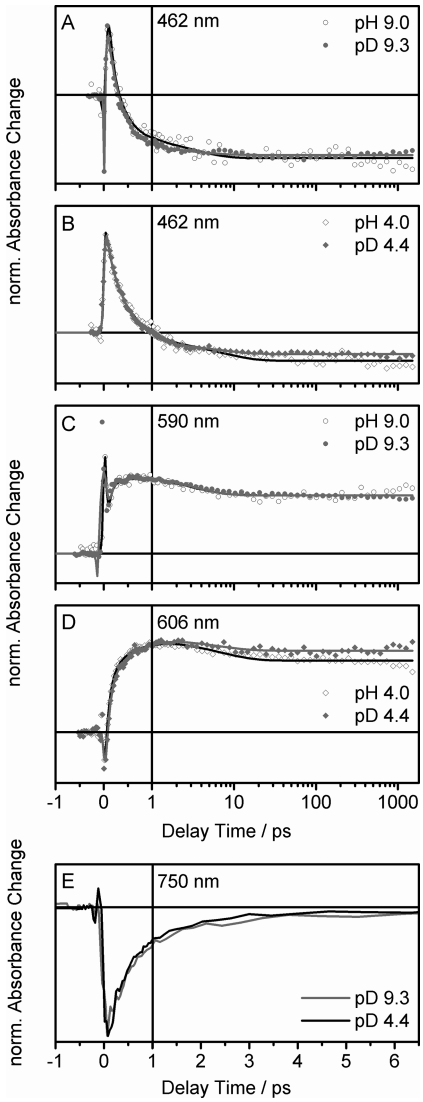

Figure 3. Transient absorbance changes of the PR D227N mutant at selected wavelengths for alkaline and acidic pH/pD values. In (A) and (B) contributions of the excited state absorption and predominantly the ground state bleaching are observed. The decay of the excited state absorption and the absorption of the photoproduct are monitored in (C) and (D). In all four plots the raw data are depicted as open and filled dots or diamonds and the global fit as solid black or gray line. In (E) the temporal evolution of the stimulated emission is compared for pD 9.3 and pD 4.4.

Because of the pH-dependent main absorption band of the retinal chromophore, the photoinduced difference spectra of PR D227N drastically differ in the spectral region between 440 and 600 nm for pH/pD 9 and pH/pD 4. Although the time resolution of the experiments performed at acidic and alkaline pH-values is approximately the same, the sub 100 fs dynamics (later on also termed coherent effect) is less pronounced at pH/pD 4. It should be noted that we cannot rule out that this signature also comprises uncorrected residuals of coherent solvent effects.

The positive signal around 480 nm arising within the cross correlation time (region (1), Figure 2B) can be again assigned to the absorption of the excited state. Compared to the transients at pH/pD 9 the signal decays considerably more slowly (Figure 3A,B). It heads to the negative contribution of

dx.doi.org/10.1021/bi3003764 | *Biochemistry* 2012, 51, 5589–5600

Table 2. Comparison of the Time Constants Obtained in the Global Fit Analysis of the PR D227N Pump/Probe Data Sets Recorded at Acidic and Alkaline pH/pD Values[a]

sample	τ_{1A}/ps	τ_{1B}/ps	τ_2/ps	τ_3/ps	τ_4
D227N, pH 9.0	0.03 ± 0.05	0.05 ± 0.05	0.28 ± 0.15	3.0 ± 1.5	infinite
D227N, pD 9.3	0.02 ± 0.05	0.02 ± 0.05	0.29 ± 0.15	3.0 ± 1.5	infinite
D227N, pH 4.0	0.08 ± 0.05		0.42 ± 0.15	6.7 ± 1.5	infinite
D227N, pD 4.4	0.08 ± 0.05		0.43 ± 0.15	6.3 ± 1.5	infinite

[a]Since under alkaline conditions strong coherent effects occur at very early delay times, two time constants < 100 fs are needed for a satisfactory description of these data sets.

the ground state bleaching signal (region (2), Figure 2B). The latter feature extends up to wavelengths of 600 nm at early delay times and is therefore drastically red-shifted compared to pH/pD 9. The positive signature of the photoproduct absorption is observed between 550 and 630 nm (region (3), Figure 2B). The signal is formed within 1 ps and partially decays with a ~5 ps time constant (Figure 3D). The maximum of this difference band is about 25 nm red-shifted compared to the one recorded under alkaline conditions. Around 700 nm again the negative signal of the stimulated emission from the S_1 state (region (4), Figure 2B) appears. Figure 3E nicely shows that the time traces of the stimulated emission and therefore the lifetimes of the excited states are equal for pD 9.3 and pD 4.4. The putative pH-dependence observed for the excited state signature must therefore be due to different superpositions of the contributions in this spectral region.

Global Fit Analyses. All data sets of the vis-pump/vis-probe experiments were fitted using eq 2. The derived time constants are displayed in Table 2. The decay times and also the decay associated spectra (DAS) are independent of the deuteration ratio (H_2O vs D_2O). Therefore, the amplitude spectra are only shown for the samples in D_2O (Figure 4).

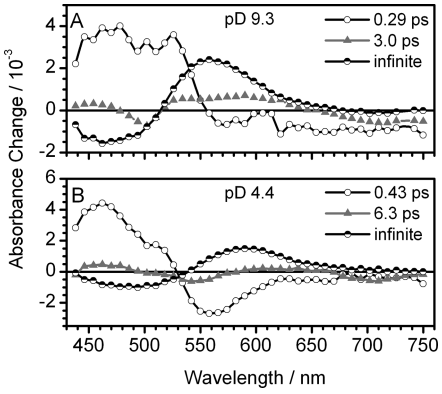

Figure 4. Decay associated spectra resulting from the global fitting procedure of the PR D227N pump/probe data sets recorded at pD 9.3 (A) and pD 4.4 (B). In each case only the spectra of the last three components are shown, since the earlier ones (τ < 0.1 ps) contain significant contributions of coherent effects around time zero.

The main dynamics for delay times >150 fs obtained at pH/pD 9 and pH/pD 4 can be described with three time constants (τ_2, τ_3, and τ_4). The last time constant thereby models the residual contributions at 1.5 ns. Because of distinct coherent signals around delay time zero at pH/pD 9 two additional time constants in the range of a few ten femtoseconds (τ_{1A}, τ_{1B}) are needed for a satisfactory description of the data sets. These ultrafast oscillatory, wavepacket-like components are considerably less pronounced at pH/pD 4. Therefore only one single sub-100 fs time constant is required for the optimal fit (τ_{1A}). Although the data have been corrected for the solvent signatures, τ_{1A} and τ_{1B} might contain coherent solvent contributions. Additionally, the observed dynamics seem to be highly nonexponential and therefore cannot be treated with the current model. The DAS of τ_{1A} and τ_{1B} are therefore neither shown nor interpreted. A further analysis of the coherent effects around time zero is given in the subsequent section.

For pD 9.3 (Figure 4A) the positive amplitude in the spectral region between 440 and 550 nm in the DAS of τ_2 = 0.29 ps must be ascribed to the decay of the excited state absorption. The accompanying negative signature (550−600 nm) is assigned to the buildup of the photoproduct. The negative amplitude at wavelengths longer than 600 nm describes the decay of the stimulated emission. Also in the DAS of τ_3 = 3.0 ps contributions of the decay of the excited state absorption (440−480 nm) and the stimulated emission (650−750 nm) are visible, pointing to a corresponding S_1 deactivation pathway. Additionally, a negative amplitude is found between 480 and 520 nm, which is attributed to the back reaction to the ground state. The spectral position of the positive signal between 520 and 650 nm coincides with the positive photoproduct difference band. A cooling process of the presumably vibrationally hot product band signature is therefore likely. The DAS of the infinite time constant reflects the signal after 1.5 ns. The difference band of the depleted ground state is monitored at 460 nm, the K-state product band at 560 nm.

For pD 4.4 (Figure 4B) the positive part of the DAS of τ_2 = 0.43 ps between 440 nm −530 nm indicates the decay of the excited state absorption. The following negative contribution until 625 nm belongs to the reformation of the ground state and/or the formation of the photoproduct. At wavelengths greater than 650 nm the decay of the stimulated emission is observed. The amplitude spectrum of τ_3 = 6.3 ps also shows the depopulation of the S_1 monitored by the decay of the excited state absorption (440 nm − 490 nm) and the stimulated emission (>650 nm). The negative signal around 550 nm most likely describes the decay of the ground state bleach. Additionally, the small positive amplitude between 580 and 640 nm points to the decay of a vibrationally hot photoproduct population. The DAS of the infinite time constant exhibits contributions of the bleached ground state population (around 480 nm) and the positive difference band of the K-photoproduct (590 nm). Obviously, these difference bands are shifted with respect to pH/pD 9.

Analysis of Coherent Effects. The characterization of the coherent effects appearing around delay time zero requires an analysis independent of the sample dynamics, since they are superimposed by the latter. To this end, a fit was applied that only describes the decay components >250 fs, which was subtracted from the transients (Figure 5A). After further data processing (see Materials and Methods), a FFT was applied

dx.doi.org/10.1021/bi3003764 | Biochemistry 2012, 51, 5589−5600

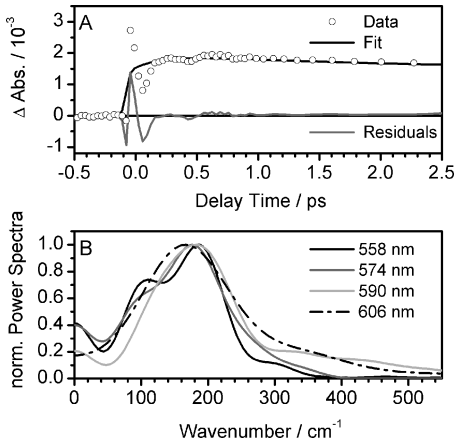

Figure 5. Transient absorbance changes of PR D227N demonstrating the unbundling of the coherent signal and the slower sample dynamics (A). The residual oscillatory signal was Fourier transformed. The resulting frequencies are shown for selected wavelengths in the region of the photoproduct absorption for pD 9.3 in (B).

and the power spectrum was evaluated. As a result of the time resolution of approximately 60 fs reliable frequencies can be resolved up to 560 cm^{-1}.

For pH 9 most pronounced coherent signals are obtained at probing wavelengths in the range of the photoproduct. The power spectra resulting from the FFT analysis show a broad distribution of frequencies in the range of 80 cm^{-1} and 300 cm^{-1} with a maximum around 160 cm^{-1} to 190 cm^{-1} (Figure 5B). The spectra arising from the blue edge of the photoproduct absorption additionally show a band around 100 cm^{-1}. The contributions at wavenumbers lower than 40 cm^{-1} are most likely unspecific. Although the coherent signals are less pronounced in the spectral region between 450 and 500 nm the obtained power spectra are quite robust and very similar to those depicted for the region of the photoproduct absorption in Figure 5B. Also here the main frequencies are in the range of 170−190 cm^{-1}.

The evaluation of the coherent signals at pH 4 is hampered by the fact that the signal size is drastically smaller compared to pH 9 and in addition the oscillations only span half a period. We thus decided not to analyze those traces any further.

Flash Photolysis Measurements. The photocycle properties of the PR D227N mutant were investigated in flash photolysis measurements at pH 9.0 (λ_{exc} = 502 nm) and pH 4.0 (λ_{exc} = 522 nm). The probing wavelengths were chosen to correspond to the absorption bands of the characteristic intermediates found in the PR wt photocycle.[12,13,19,21,23] The band at 400 nm is indicative for the M-intermediate and around 500 nm the ground state bleaching signal appears (Figure 6A,C). Around 570 nm the absorption of the K-intermediate is visible, and the absorption of the late intermediates can be monitored at 610 nm (Figure 6B,D). In order to correlate the observed kinetics to specific processes in the photocycle a global fitting routine using a sum of exponential functions (eq 2) was applied to each data set. A satisfactory description of the transients requires five time constants at pH 9.0 and six time constants at pH 4.0 (Table 3).

At pH 9.0, the positive absorbance change of the K-intermediate is visible at 560 and 610 nm directly after photoexcitation (Figure 6B). It decays with time constants of τ_1 = 20 μs and τ_2 = 170 μs. Concomitantly, an absorbance increase is monitored at 400 nm (Figure 6A). It is assigned to

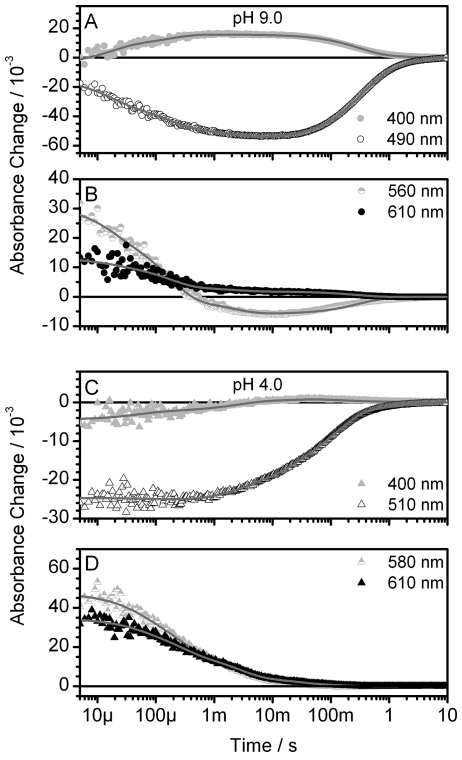

Figure 6. Transient absorbance changes of the PR D227N mutant under alkaline (circles, A and B) and acidic conditions (triangles, C and D). The raw data are plotted as open or filled symbols, the global fits of each data set as solid gray lines. The transients are indicative of the formation of the blue-shifted M-like intermediate (400 nm), the ground state bleach (490 nm, 510 nm) as well as the early K and the late (N/O-like) intermediates (560 nm/580 nm, 610 nm).

the M-intermediate formation with its deprotonated Schiff base configuration. Afterward the transient at 400 nm reaches a plateau ranging from 1 to 50 ms. During this time period the first small signature of the late red-shifted intermediates is visible (Figure 6B). Figure 6A indicates that the ground state recovers with a main time constant in the range of τ_5 = 300 ms and a further slower component (τ_6 = 2 s). Surprisingly, a 400 nm signal can be observed up to the end of the photocycle. The decay of the late red-shifted states is also visible in this time range.

The transient absorbance changes at pH 4.0 reveal a considerably different photocycle behavior (Figure 6C,D). The K-intermediate decays on a slower time scale (τ_1 = 50 μs, τ_2 = 250 μs) compared to pH 9.0. In accordance with other flash photolysis studies of PR wt the photocycle of the D227N mutant does not exhibit a contribution of the blue-shifted M-intermediate at pH 4.0. The slightly negative signal at early times most likely corresponds to the bleaching of the $S_0 \rightarrow S_2$ transition of the ground state. The small absorbance change of the late red-shifted intermediates accompanies the decay of the K-state; no formation kinetics can be monitored (Figure 6D). At pH 4 the ground state is recovered with three time contstants (see 510 nm transient in Figure 6C).

DISCUSSION

pH-Titration. The neutralization of the charge at position 227 already affects the ground state absorption properties of the chromophore. At pH 9, the main retinal band shifts from approximately 520 nm in the wt[13] to 502 nm in the D227N

dx.doi.org/10.1021/bi3003764 | Biochemistry 2012, 51, 5589−5600

Table 3. Comparison of the Time Constants Obtained in the Global Fit Analysis of the PR D227N Flash Photolysis Data Sets at pH 9.0 and 4.0

sample	τ_1 (μs)	τ_2 (μs)	τ_3 (ms)	τ_4 (ms)	τ_5 (ms)	τ_6 (s)
D227N, pH 9.0	20 ± 10	170 ± 50	2.0 ± 0.5		300 ± 50	2 ± 1
D227N, pH 4.0	50 ± 10	250 ± 50	3.0 ± 0.5	23 ± 5	150 ± 50	2 ± 1

mutant (Figure 1). This spectral blue-shift of approximately 20 nm is attributed to the altered charge and H-bond distribution in the immediate vicinity of the chromophore.

At low pH, the main absorption band of the D227N mutant shifts to 520 nm (pH 5.0). As for PR wt this effect is attributed to the fact that the charged primary proton acceptor Asp97 influences the potential energy surfaces of the protein. With 18 nm, the pH-induced spectral change of the main band is somewhat less pronounced than in PR wt (28 nm).[13] The evaluation of the pH-dependent position of the absorption maximum permits the determination of the pK_a value of Asp97 (Figure 1D). With a mean value of 6.25 the pK_a was found to be lower than the one observed for the wt (pK_a(PR wt) = 7.0–8.2).[12,13,25] This finding nicely corroborates the results obtained by Imasheva et al.[30]

In the D227N mutant, the intensity of the main retinal band decreases with increasing pH-values (Figure 1B,C). This is probably because not only the side chain of Asp97 is titrated within the pH range used, but also the Schiff base. The recorded UV–vis spectra show the concomitant formation of a further band peaking at 368 nm. Here, also a pH-induced shift is monitored. The band peaks at 368 nm under alkaline conditions and is found at 389 nm at pH 5. Because of its spectral position this band can be assigned to a retinal with a deprotonated Schiff base. Also the $S_0 \rightarrow S_2$ absorption band of the retinal is found at this position. Part of the signal therefore might also be traced back to the retinal beta-band. Finally also there is the 13-*cis* form of the retinal, which is supposed to have a higher extinction coefficient than the all-*trans* band might contribute. The evaluation of the pH-induced rise of the UV-band yields a typical titration curve with its sigmoidal shape. We infer from this result the deprotonation reaction of the Schiff base as the most likely explanation. The respective pK_a value was determined to be 7.4. NMR measurements could not observe resonances in PR wt indicative for the deprotonated Schiff base below pH 12.[41] The pK_a of the Schiff base is therefore drastically reduced by the D227N mutation. First solid-state NMR data on D227N revealed 15N chemical shift changes of D227N compared to wild type PR indicating a direct effect of this mutation on the Schiff base properties (Hempelmann et al., Supporting Information[27]). In summary, the results of the titrations lead to the conclusion that the loss of the charge and accordingly the loss of the water binding site at Asp227 stabilize the deprotonated forms of both Asp97 and the Schiff base.

Isomeric Composition of the D227N Samples. Retinal extraction experiments were performed prior to the time-resolved experiments in order to quantify the chromophore species excited. The HPLC traces of the extracted chromophore isomers were assigned according to the available retinal standards (all-*trans*, 13-*cis*, 9-*cis*) measured under identical conditions. As a further control we also extracted retinal from PR wt samples. The outcome of the wt experiments coincides with previously published results.[13] The obtained retention times of the standards perfectly match those of the extracted PR D227N samples. At acidic pH-values the isomeric ratio was determined to be roughly 76% all-*trans* and 22% 13-*cis*. In the alkaline environment the ratio is approximately 67% all-*trans* and 32% 13-*cis*. The fraction of the remaining isomer (presumably 9-*cis*) is <2%. This finding differs from previous studies by Imesheva et al.,[42] which found a considerable amount of 11-*cis* retinal at pH 8.5. The deviations could arise from the different samples that were used (C107V/C156V/C175V/D227N vs D227N), which may lead to a modified retinal binding pocket where other isomers are stabilized.

Since the absorption spectra of the different retinal isomers incorporated in PR are unknown so far, it is not unambiguously clear which isomer is excited in the time-resolved measurements. Because of the high fraction of all-*trans* retinal, we assume that the reaction dynamics predominantly originates from the excitation of this isomer. Contributions of a 13-*cis* photocycle cannot be excluded. However, the absorption maximum of 13-*cis* retinal included in PR should most likely differ from the one of the embedded all-*trans* isomer. Additionally, the extinction coefficient is supposed to be lower for 13-*cis* retinal. On that account, we neglect a simultaneous 13-*cis* excitation.

Model of Retinal Isomerization in D227N. The analysis of the vis-pump/vis-probe data recorded for the D227N mutant shows that independent of the deuteration ratio as well as the pH/pD value (9 vs 4) the same general reaction steps are observed. Since those nicely conform to the findings of PR wt,[17,18,43] they can be interpreted within the framework of the reaction model derived for wt.[17] The reaction cycle is started by the excitation of the all-*trans* retinal chromophore to the S_1 potential energy surface. The shortest time constant of less than 150 fs has been ascribed to a wavepacket motion out of the Franck–Condon region. Lenz et al. suggested that a nuclear stretch motion is connected to this process. Also the global fit of the D227N data revealed very short time constants, in this case below 100 fs. Because of the better time resolution of the present study the data at the early delay times are superimposed by coherent effects. Fourier analysis of these effects show low frequency vibrations between 80 cm^{-1} and 300 cm^{-1}, which peak around 175 cm^{-1}. Besides multiple torsional modes that are active below 300 cm^{-1} in the reactive excited states of retinal proteins,[44,45] Kahan et al. especially claim the 170 cm^{-1} vibration to be due to the symmetric in-plane motion of the retinal.[38] In an ultrafast Kerr shutter fluorescence measurement of PR wt it was shown that a dynamic Stokes shift is connected to the processes observed within the first 200 fs.[17] Our transient data recorded on the D227N mutant show a similar effect: A strong red-shift of the stimulated emission band is monitored within the first 200 fs.

The retinal stretching is followed by a torsional motion in the 300 fs time range, in other words the formation of a twisted, photoproduct-like retinal configuration, which leads to the CI with the ground state. The DAS of the time constants τ_2 indicates contributions of photoproduct formation for the D227N mutant at both pH/pD values. As for the wt, the transition to the electronic ground state proceeds biexponentially via two decay channels (τ_2 and τ_3) in PR D227N. Lenz et

dx.doi.org/10.1021/bi3003764 | Biochemistry 2012, 51, 5589–5600

al. explained this finding with the hypothesis that not all of the molecules reach the CI directly, but some have to overcome a barrier. At the ground state PES the molecules can either go back to the all-*trans* configuration or decay to the 13-*cis* conformation. For PR D227N the DAS of τ_3 supports the presence of such a back reaction. At the end of the investigated time range the PR_K-PR difference spectrum with its relaxed red-shifted photoproduct signature is observed.

pH-dependence of the Primary Reaction. For PR wt and several mutants, for example, His75 mutants, the excited state deactivation is drastically dependent on the pH-value.[17,27,29,46] The time constants derived in the present study of the PR D227N mutant also show a small pH-dependence (Table 2). This small pH-sensitivity can be visualized best in the individual transient absorbance changes which are indicative for the decay of the excited state absorption (Figure 3A,B). However, a comparison of the time traces of the stimulated emission which are not perturbed by overlapping contributions of the ground state bleach and the absorption of the excited state and/or the photoproduct (λ_{Probe} > 650 nm) reveals identical temporal evolution at pD 4.4 and pD 9.3 within the signal-to-noise ratio (Figure 3E). The modeled small pH-dependence of the global time constants must therefore originate from the different spectral shifts of the contributions observed at pH/pD 9 and pH/pD 4. It can thus be concluded that the pH-dependence of the primary dynamics is lost if Asp227 is replaced by Asn.

A comparison of the S_1 deactivation time constants (τ_2 and τ_3) determined for the D227N mutant with those of the wt[17,29,46] shows that they are very similar to the values obtained for PR wt with a deprotonated Asp97 (pH 9). On the contrary, the decay times obtained for the wt under acidic conditions are considerably larger. This shows again that the photocycle of PR is not optimized for speed.[27] In conclusion, this means that the primary reaction is not only determined by the charge at the primary proton acceptor but also the interplay of the charges at Asp97 and Asp227. Additionally, also the interacting hydrogen bonding network around the Schiff base in the binding pocket must be of considerable importance for the excited state deactivation pathways.

Kinetic Isotope Effect of the Excited State Deactivation. For PR D227N, the comparison of the individual transient absorbance changes measured in D_2O and H_2O reveals under both alkaline and acidic conditions no significant differences in the dynamics dependent on the deuteration level. Consequently, the obtained time constants and the respective DAS are identical within the experimental accuracy for pH 9.0 and pD 9.3 as well as pH 4.0 and pD 4.4.

This finding clearly differs from the results obtained for PR wt and the D97N mutant.[18,47] For PR wt a kinetic isotope effect of 2.4 was calculated at pH/pD 9. It decreases to a kinetic isotope effect of 1.6 at pH/pD 6 and is with a value of 1.3 even less pronounced for the D97N mutant. The different values for the kinetic isotope effect have been explained by the absence of a catalytic water molecule in the vicinity of the counterion complex and the Schiff base for the wt protein at pH 6 and the D97N mutant. The FTIR measurements of Ikeda et al. demonstrate that also the removal of the negative charge at position 227 in PR D227N leads to the lack of a strongly hydrogen-bounded water in the vicinity of Asp97, Asp227, and the Schiff base.[28] Similar observations were also made for the respective BR mutants D85N and D212N.[48,49] In conclusion, our femtosecond-transient absorption measurements carried out in H_2O and D_2O further prove that the negative charge of Asp227 is one of the main determinants of the H-bonding pattern in the retinal binding pocket.

The Slower Photocycle Dynamics. The subsequent photocycle steps which are triggered by the isomerization process were investigated using the flash photolysis technique. The general sequence of intermediates is analogous to the results obtained for PR wt.[12,13,19,21,23,27] At alkaline pH the prominent signature of the K-state is followed by the formation of the blue-shifted M-intermediate (τ_1 = 20 μs, τ_2 = 170 μs). At the end of the reaction cycle slightly red-shifted intermediate(s) are observed, which decay with a main contribution of τ_5 = 300 ms. Under acidic conditions also the early K-state and the late red-shifted states are successively monitored. A formation dynamics of the latter is not visible since it is superimposed by the decay of the K-state. Like for PR wt, the M-intermediate is not detectable under these conditions.

Besides these general agreements several pronounced differences to the PR wt photocycle are observed. Independent of the pH, the most outstanding feature of the PR D227N reaction cycle is its exceedingly long duration. At acidic as well as at alkaline pH-values turnover rates of 0.5 s^{-1} (τ_6 = 2 s) have been modeled. This is in both cases more than 10 times slower than for PR wt (compare to ref 27 since the preparation of the wt sample is equal to the one used for the D227N mutant). Interestingly, the τ_6 = 2 s does not describe the main ground state recovery channel. The process attributed to τ_5 is clearly the dominant deactivation pathway (Figure 6A,C). Contrary to the last decay constant τ_5 exhibits a clear pH-dependence (τ_5 (pH 9) = 300 ms, τ_5 (pH 6) = 150 ms). This result is in good agreement with measurements of PR wt,[27] which showed the photocycle at alkaline pH to be approximately a factor of 2 slower.

A closer look at the transient absorbance changes indicative for the ground state recovery demonstrates a further difference between the photocycle at pH 4.0 and pH 9.0. At pH 4.0 a third time constant is needed to model the ground state recovery. This decay time of τ_4 = 23 ms is not required to describe the alkaline dynamics. This finding is in opposition to the photocycle dynamics of PR wt or the His75 mutants,[27] since for these data sets one extra time constant is needed to model the data recorded under alkaline conditions. Another important difference between PR wt and its D227N mutant in the alkaline environment is the negligibly small signal of the N/O intermediates for the mutant. Most likely these states cannot be accumulated due to the decrease of the Schiff base pK_a in the photointermediates and accordingly the slow decay of the M-state.

Moreover, the alkaline photocycle of PR D227N itself possesses one additional striking feature. Unlike other retinal proteins, the M-state is present until the end of the reaction cycle. This has neither been observed for the wt protein nor for the His75 mutations of PR.[13,19,21,26,27] It is most likely connected to the fact that the D227N mutation strongly affects the H-bonding character of the Schiff base.[28] It seems that the mutation does not only lower the pK_a of the Schiff base in the unphotolyzed ground state, but also an efficient reprotonation reaction could not be observed. Further electrophysiological and kinetic studies are necessary to fully understand the function of Asp227 concerning the relevance of its negative charge as well as its implications on the hydrogen bonding network in the retinal binding pocket. The present

dx.doi.org/10.1021/bi3003764 | *Biochemistry* 2012, 51, 5589−5600

results already highlight its critical role for all steps of the PR photocycle.

Comparison to the Homologous BR Mutant. In BR, the homologous position of Asp227 in PR is also occupied by an Asp residue (in BR Asp212). In the ground state BR Asp212 exists in its ionized, deprotonated form[50] as PR Asp227. Together with Arg82 and Asp85, Asp212 is part of the Schiff base counterion complex in the retinal binding pocket of BR. It also plays a relevant role in the proton pumping mechanism. This residue is for example involved in the primary proton transfer from the Schiff base to Asp85 upon formation of the M intermediate.[51] Also the restoration of the charge at Asp85 at the end of the photocycle (O intermediate) proceeds via Asp212.[52,53] Accordingly, no net charge translocation occurs in the entire pH range from 0 up to 11.[54] However, it could be demonstrated, that upon addition of chloride, the net proton pumping is restored from pH 3.8 to 7.2. Outside this pH range, transient charge motion similar to the acid-blue to acid-purple transition of wt BR takes place.[55]

For PR D227N our results as well as former studies[30,42] show that the visible absorption maximum is approximately 20 nm blue-shifted compared to PR wt. Using *Escherichia coli* as the expression system (like for PR) results in a similar shift for BR and the respective mutant D212N.[54,56] However, this blue-shift is controversial to the predicted red-shift after removal of a negative charge according to the point-charge-model of rhodopsins.[57] Indeed, when expressed in the natural host *Halobacterium salinarum*, the D212N mutant of BR exhibits a large red-shift.[58] As suggested by Shibata et al.,[59] this discrepancy may be indicative for an unusual protein folding resulting in modified properties of BR. Furthermore, the presence of halide anions has been shown to generate a hypsochromically shifted absorption of the main retinal band in BR D212N.[59] The pH-dependent UV−vis spectra additionally show that the pK_a of the Schiff base is drastically reduced by the PR D227N mutation. For BR such an effect is well-known for the counterion mutant BR D85N.[60,61]

The BR D212N mutation has also a high impact on the photocycle properties of BR. Already the primary reaction steps, that is, retinal isomerization, show significant deviations compared to the wt. The decay of the S_1 state has shown to be biexponential in the D212N mutant at pH 5,[62] whereas a monoexponential deactivation of the excited state (in both cases exclusive of the ultrafast sub 150 fs component) has been observed for BR wt.[63−65] Also the reaction rates vary: The lifetime of the excited state is four times higher in the mutant ($\tau_{BR\ wt} \approx 0.5$ ps; $\tau_{BR\ D212N} = 2$ ps (and 6 ps)). Halides, in this case Cl^-, have a decisive influence on the excited state deactivation pathway.[66] Adding 1 M NaCl to the BR D212N sample significantly accelerates the S_1 decay ($\tau_{BR\ D212N,\ NaCl} = 1$ ps), which was found to become monoexponential. In the present study of PR D227N no decelerated dynamics compared to PR wt was found. Like in PR wt the mutated protein exhibits a biexponential deactivation characteristics of the excited state. The first time constant describing the S_1 decay is thereby in the range of the value obtained for the PR wt under alkaline conditions.[17] The second one is even smaller compared to the wild type. Owing to the presence of 100 mM NaCl in our buffer solution, an effect of chloride ions cannot be precluded. At least, Sharaabi et al. showed for PR wt that the pK_a value of Asp97 exhibits a small NaCl dependence (7.8 in deionized water, 7.0 after adding 300 mM NaCl).[67] Additionally they suggest that also the M intermediate decay at pH 9.4 might be influenced by the salt concentration. Since the electrostatic changes within the retinal binding pocket are supposed to be the same in the BR D212N and PR D227N mutations, the observed differences in the primary reaction dynamics can most likely be explained by a considerably altered hydrogen bonding characteristiscs for both proteins. Indeed Ikeda et al. could show that upon isomerization the Schiff base forms a strong hydrogen bond in PR (interaction with Asp227) which was not observed for BR.[28]

Also the subsequent dynamics of PR D227N differs considerably from the one of the respective BR mutant. For PR the mutation of Asp227 results in a dominant, long-lived M-like state and a considerably elongated photocycle. However, for BR D212N at pH-values <7 the amount of the M state is drastically reduced to 15%; at pH-values >7 it is not even detected.[58] For all stated reasons, the effect of the neutralized charge at position 227 in PR (212 in BR) differs drastically for PR and BR. A part of these differences is most probably caused by the varying H-bonding characteristics around the Schiff base and the counterion complex in BR and PR. It may also be the case that Asp227 in PR and Asp212 in BR possess slightly different functions in the photocycle. Exactly these highlighted differences between the mutations in BR and PR make the PR D227N mutant an important PR variant for further research.

AUTHOR INFORMATION

Corresponding Author

*Phone: +49 69 798 29351. Fax: +49 69 798 29709. E-mail: wveitl@theochem.uni-frankfurt.de.

Funding

This work has been funded by the DFG via the SFB 807 "Transport and Communications across Biological Membranes" and the Cluster of Excellence Frankfurt "Macromolecular Complexes".

Notes

The authors declare no competing financial interest.

ACKNOWLEDGMENTS

We thank Christian Czech for his contributions to the titration experiments. Dr. Nina Gildenhoff and Frank Scholz are acknowledged for experimental support.

ABBREVIATIONS:

BR, bacteriorhodopsin; CI, conical intersection; DAS, decay associated spectrum; DDM, *n*-dodecyl-*β*-D-maltoside; FFT, fast Fourier transformation; NOPA, noncollinear optical parametric amplifier; PR, proteorhodopsin; TRIS, tris(hydroxymethyl)-aminomethane

REFERENCES

(1) Béjà, O., Aravind, L., Koonin, E. V., Suzuki, M. T., Hadd, A., Nguyen, L. P., Jovanovich, S., Gates, C. M., Feldman, R. A., Spudich, J. L., Spudich, E. N., and DeLong, E. F. (2000) Bacterial rhodopsin: Evidence for a new type of phototrophy in the sea. *Science 289*, 1902−1906.

(2) Nagel, G., Ollig, D., Fuhrmann, M., Kateriya, S., Mustl, A. M., Bamberg, E., and Hegemann, P. (2002) Channelrhodopsin-1: A light-gated proton channel in green algae. *Science 296*, 2395−2398.

(3) Nagel, G., Szellas, T., Huhn, W., Kateriya, S., Adeishvili, N., Berthold, P., Ollig, D., Hegemann, P., and Bamberg, E. (2003) Channelrhodopsin-2, a directly light-gated cation-selective membrane channel. *Proc. Natl. Acad. Sci. U. S. A. 100*, 13940−13945.

(4) Oesterhelt, D. (1998) The structure and mechanism of the family of retinal proteins from halophilic archaea. *Curr. Opin. Struct. Biol. 8*, 489−500.
(5) Oesterhelt, D., and Stoeckenius, W. (1971) Rhodopsin-like protein from purple membrane of halobacterium-halobium. *Nat. New. Biol. 233*, 149−152.
(6) Ridge, K. D., and Palczewski, K. (2007) Visual rhodopsin sees the light: structure and mechanism of G protein signaling. *J. Biol. Chem. 282*, 9297−9301.
(7) Scharf, B., Pevec, B., Hess, B., and Engelhard, M. (1992) Biochemical and photochemical properties of the photophobic receptors from Halobacterium halobium and Natronobacterium pharaonis. *Eur. J. Biochem. 206*, 359−366.
(8) Spudich, J. L., Yang, C. S., Jung, K. H., and Spudich, E. N. (2000) Retinylidene proteins: structures and functions from archaea to humans. *Annu. Rev. Cell Dev. Biol. 16*, 365−392.
(9) Man, D. L., Wang, W. W., Sabehi, G., Aravind, L., Post, A. F., Massana, R., Spudich, E. N., Spudich, J. L., and Béjà, O. (2003) Diversification and spectral tuning in marine proteorhodopsins. *EMBO J. 22*, 1725−1731.
(10) Reckel, S., Gottstein, D., Stehle, J., Löhr, F., Verhoefen, M.-K., Takeda, M., Silvers, R., Kainosho, M., Glaubitz, C., Wachtveitl, J., Bernhard, F., Schwalbe, H., Güntert, P., and Dötsch, V. (2011) Solution NMR Structure of Proteorhodopsin. *Angew. Chem., Int. Ed. Engl. 50*, 11942−11946.
(11) Bergo, V., Amsden, J. J., Spudich, E. N., Spudich, J. L., and Rothschild, K. J. (2004) Structural changes in the photoactive site of proteorhodopsin during the primary photoreaction. *Biochemistry 43*, 9075−9083.
(12) Dioumaev, A. K., Brown, L. S., Shih, J., Spudich, E. N., Spudich, J. L., and Lanyi, J. K. (2002) Proton transfers in the photochemical reaction cycle of proteorhodopsin. *Biochemistry 41*, 5348−5358.
(13) Friedrich, T., Geibel, S., Kalmbach, R., Chizhov, I., Ataka, K., Heberle, J., Engelhard, M., and Bamberg, E. (2002) Proteorhodopsin is a light-driven proton pump with variable vectoriality. *J. Mol. Biol. 321*, 821−838.
(14) Abramczyk, H. (2004) Femtosecond primary events in bacteriorhodopsin and its retinal modified analogs: Revision of commonly accepted interpretation of electronic spectra of transient intermediates in the bacteriorhodopsin photocycle. *J. Chem. Phys. 120*, 11120−11132.
(15) Haupts, U., Tittor, J., and Oesterhelt, D. (1999) Closing in on bacteriorhodopsin: Progress in understanding the molecule. *Annu. Rev. Biophys. Biomol. Struct. 28*, 367−399.
(16) Lanyi, J. K. (2000) Molecular mechanism of ion transport in bacteriorhodopsin: Insights from crystallographic, spectroscopic, kinetic, and mutational studies. *J. Phys. Chem. B 104*, 11441−11448.
(17) Lenz, M. O., Huber, R., Schmidt, B., Gilch, P., Kalmbach, R., Engelhard, M., and Wachtveitl, J. (2006) First steps of retinal photoisomerization in proteorhodopsin. *Biophys. J. 91*, 255−262.
(18) Neumann, K., Verhoefen, M.-K., Weber, I., Glaubitz, C., and Wachtveitl, J. (2008) The initial reaction dynamics of proteorhodopsin observed by femtosecond infrared and visible spectroscopy. *Biophys. J. 94*, 4796−4807.
(19) Váró, G., Brown, L. S., Lakatos, M., and Lanyi, J. K. (2003) Characterization of the photochemical reaction cycle of proteorhodopsin. *Biophys. J. 84*, 1202−1207.
(20) Xiao, Y. W., Partha, R., Krebs, R., and Braiman, M. (2005) Time-resolved FTIR spectroscopy of the photointermediates involved in fast transient H^+ release by proteorhodopsin. *J. Phys. Chem. B 109*, 634−641.
(21) Lakatos, M., and Váró, G. (2004) The influence of water on the photochemical reaction cycle of proteorhodopsin at low and high pH. *J. Photochem. Photobiol. B 73*, 177−182.
(22) Ranaghan, M. J., Schwall, C. T., Alder, N. N., and Birge, R. R. (2011) Green proteorhodopsin reconstituted into nanoscale phospholipid bilayers (nanodiscs) as photoactive monomers. *J. Am. Chem. Soc. 133*, 18318−18327.
(23) Lakatos, M., Lanyi, J. K., Szakács, J., and Váró, G. (2003) The photochemical reaction cycle of proteorhodopsin at low pH. *Biophys. J. 84*, 3252−3256.
(24) Lörinczi, É., Verhoefen, M.-K., Wachtveitl, J., Wörner, A. C., Glaubitz, C., Engelhard, M., Bamberg, E., and Friedrich, T. (2009) Voltage- and pH-dependent changes in vectoriality of photocurrents mediated by wild-type and mutant proteorhodopsins upon expression in xenopus. *J. Mol. Biol. 393*, 320−341.
(25) Krebs, R. A., Dunmire, D., Partha, R., and Braiman, M. S. (2003) Resonance Raman characterization of proteorhodopsin's chromophore environment. *J. Phys. Chem. B 107*, 7877−7883.
(26) Bergo, V. B., Sineshchekov, O. A., Kralj, J. M., Partha, R., Spudich, E. N., Rothschild, K. J., and Spudich, J. L. (2009) His-75 in proteorhodopsin, a novel component in light-driven proton translocation by primary pumps. *J. Biol. Chem. 284*, 2836−2843.
(27) Hempelmann, F., Hölper, S., Verhoefen, M.-K., Wörner, A., Köhler, T., Fiedler, S.-A., Pfleger, N., Wachtveitl, J., and Glaubitz, C. (2011) The His75-Asp97 cluster in green proteorhodopsin. *J. Am. Chem. Soc. 133*, 4645−4654.
(28) Ikeda, D., Furutani, Y., and Kandori, H. (2007) FTIR study of retinal Schiff base and internal water molecules of proteorhodopsin. *Biochemistry 46*, 5365−5373.
(29) Rupenyan, A., van Stokkum, I. H. M., Arents, J. C., van Grondelle, R., Hellingwerf, K., and Groot, M. L. (2008) Characterization of the primary photochemistry of proteorhodopsin with femtosecond spectroscopy. *Biophys. J. 94*, 4020−4030.
(30) Imasheva, E. S., Balashov, S. P., Wang, J. M., Dioumaev, A. K., and Lanyi, J. K. (2004) Selectivity of retinal photoisomerization in proteorhodopsin is controlled by aspartic acid 227. *Biochemistry 43*, 1648−1655.
(31) Scherrer, P., Mathew, M. K., Sperling, W., and Stoeckenius, W. (1989) Retinal isomer ratio in dark-adapted purple membrane and bacteriorhodopsin monomers. *Biochemistry 28*, 829−834.
(32) Seltzer, S. (1992) Solvent isotope effects on retinal cis-trans isomerization in the dark adaptation of bacteriorhodopsin. *J. Am. Chem. Soc. 114*, 3516−3520.
(33) Nishikawa, T., Murakami, M., and Kouyama, T. (2005) Crystal structure of the 13-cis isomer of bacteriorhodopsin in the dark-adapted state. *J. Mol. Biol. 352*, 319−328.
(34) Hubbard, R., Brown, P. K., and Bownds, D. (1971) Methodology of vitamin A and visual pigments. *Methods Enzymol. 18C*, 615−653.
(35) Riedle, E., Beutter, M., Lochbrunner, S., Piel, J., Schenkl, S., Spörlein, S., and Zinth, W. (2000) Generation of 10 to 50 fs pulses tunable through all of the visible and the NIR. *Appl. Phys. B: Laser Opt. 71*, 457−465.
(36) Wynne, K., Haran, G., Reid, G. D., Moser, C. C., Dutton, P. L., and Hochstrasser, R. M. (1996) Femtosecond infrared spectroscopy of low-lying excited states in reaction centers of Rhodobacter sphaeroides. *J. Phys. Chem. 100*, 5140−5148.
(37) Kovalenko, S. A., Dobryakov, A. L., Ruthmann, J., and Ernsting, N. P. (1999) Femtosecond spectroscopy of condensed phases with chirped supercontinuum probing. *Phys. Rev. A 59*, 2369−2384.
(38) Kahan, A., Nahmias, O., Friedman, N., Sheves, M., and Ruhman, S. (2007) Following photoinduced dynamics in bacteriorhodopsin with 7-fs impulsive vibrational spectroscopy. *J. Am. Chem. Soc. 129*, 537−546.
(39) Wang, Q., Schoenlein, R. W., Peteanu, L. A., Mathies, R. A., and Shank, C. V. (1994) Vibrationally coherent photochemistry in the femtosecond primary event of vision. *Science 266*, 422−424.
(40) Verhoefen, M. K., Bamann, C., Blöcher, R., Förster, U., Bamberg, E., and Wachtveitl, J. (2010) The photocycle of channelrhodopsin-2: Ultrafast reaction dynamics and subsequent reaction steps. *ChemPhysChem 11*, 3113−3122.
(41) Pfleger, N., Lorch, M., Wörner, A. C., Shastri, S., and Glaubitz, C. (2008) Characterisation of Schiff base and chromophore in green proteorhodopsin by solid-state NMR. *J. Biomol. NMR 40*, 15−21.
(42) Imasheva, E. S., Shimono, K., Balashov, S. P., Wang, J. M., Zadok, U., Sheves, M., Kamo, N., and Lanyi, J. K. (2005) Formation of

a long-lived photoproduct with a deprotonated Schiff base in proteorhodopsin, and its enhancement by mutation of Asp227. *Biochemistry 44*, 10828−10838.
(43) Huber, R., Satzger, H., Zinth, W., and Wachtveitl, J. (2001) Noncollinear optical parametric amplifiers with output parameters improved by the application of a white light continuum generated in CaF_2. *Opt. Commun. 194*, 443−448.
(44) Cembran, A., Bernardi, F., Olivucci, M., and Garavelli, M. (2003) Excited-state singlet manifold and osciallatory features of a ninatetraeniminium retinal chromophore model. *J. Am. Chem. Soc. 125*, 12509−12519.
(45) Lin, S. W., Groesbeek, M., van der Hoef, I., Verdegem, P., Lugtenburg, J., and Mathies, R. A. (1998) Vibrational assignment of torsional normal modes of rhodopsin: Probing excited-state dynamics along the reactive C_{11}=C_{12} torsional coordinate. *J. Phys. Chem. B 102*, 2787−2806.
(46) Huber, R., Köhler, T., Lenz, M. O., Bamberg, E., Kalmbach, R., Engelhard, M., and Wachtveitl, J. (2005) pH-dependent photoisomerization of retinal in proteorhodopsin. *Biochemistry 44*, 1800−1806.
(47) Verhoefen, M. K., Neumann, K., Weber, I., Glaubitz, C., and Wachtveitl, J. (2009) Primary reaction dynamics of proteorhodopsin mutant D97N observed by femtosecond infrared and visible spectroscopy. *Photochem. Photobiol. 85*, 540−546.
(48) Shibata, M., Tanimoto, T., and Kandori, H. (2003) Water molecules in the Schiff base region of bacteriorhodopsin. *J. Am. Chem. Soc. 125*, 13312−13313.
(49) Shibata, M., and Kandori, H. (2005) FTIR studies of internal water molecules in the Schiff base region of bacteriorhodopsin. *Biochemistry 44*, 7406−7413.
(50) Braiman, M. S., Mogi, T., Marti, T., Stern, L. J., Khorana, H. G., and Rothschild, K. J. (1988) Vibrational spectroscopy of bacteriorhodopsin mutants - light-driven proton transport involves protonation changes of aspartic-acid residue-85, residue-96, and residue-212. *Biochemistry 27*, 8516−8520.
(51) Tanimoto, T., Furutani, Y., and Kandori, H. (2003) Structural changes of water in the Schiff base region of bacteriorhodopsin: A proposal of a hydration switch Model. *Biochemistry 42*, 2300−2306.
(52) Dioumaev, A. K., Brown, L. S., Needleman, R., and Lanyi, J. K. (1999) Fourier transform infrared spectra of a late intermediate of the bacteriorhodopsin photocycle suggest transient protonation of Asp-212. *Biochemistry 38*, 10070−10078.
(53) Zscherp, C., Schlesinger, R., and Heberle, J. (2001) Time-resolved FT-IR spectroscopic investigation of the pH-dependent proton transfer reactions in the E194Q mutant of bacteriorhodopsin. *Biochem. Biophys. Res. Commun. 283*, 57−63.
(54) Mogi, T., Stern, L. J., Marti, T., Chao, B. H., and Khorana, H. G. (1988) Aspartic acid substitutions affect proton translocation by bacteriorhodopsin. *Proc. Natl. Acad. Sci. U. S. A. 85*, 4148−4152.
(55) Moltke, S., Krebs, M. P., Mollaaghababa, R., Khorana, H. G., and Heyn, M. P. (1995) Intramolecular charge transfer in the bacteriorhodopsin mutants Asp85-->Asn and Asp212-->Asn: effects of pH and anions. *Biophys. J. 69*, 2074−2083.
(56) Stern, L. J., Ahl, P. L., Marti, T., Mogi, T., Duiiach, M., Berkowitz, S., Rothschild, K. J., and Khorana, H. G. (1989) Substitution of membrane-embedded aspartic acids in bacteriorhodopsin causes specific changes in different steps of the photochemical cycle. *Biochemistry 28*, 10035−10042.
(57) Honig, B., Dinur, U., Nakanishi, K., Balogh-Nair, V., Gawinowicz, M. A., Arnaboldi, M., and Motto, M. G. (1979) An external point-charge model for wavelength regulation in visual pigments. *J. Am. Chem. Soc. 101*, 7084−7086.
(58) Needleman, R., Chang, M., Ni, B., Váró, G., Fornés, J., White, S. H., and Lanyi, J. K. (1991) Properties of Asp212Asn bacteriorhodopsin suggest that Asp212 and Asp96 both participate in a counterion and proton acceptor complex near the Schiff base. *J. Biol. Chem. 266*, 11478−11484.
(59) Shibata, M., Yoshitsugu, M., Mizuide, N., Ihara, K., and Kandori, H. (2007) Halide binding by the D212N mutant of bacteriorhodopsin affects hydrogen bonding of water in the active site. *Biochemistry 46*, 7525−7535.
(60) Otto, H., Marti, T., Holz, M., Mogi, T., Stern, L. J., Engel, F., Khorana, H. G., and Heyn, M. P. (1990) Substitution of amino acids Asp-85, Asp-212, and Arg-82 in bacteriorhodopsin affects the proton release phase of the pump and the pK of the Schiff base. *Proc. Natl. Acad. Sci. U. S. A. 87*, 1018−1022.
(61) Tittor, J., Schweiger, U., Oesterhelt, D., and Bamberg, E. (1994) Inversion of proton translocation in bacteriorhodopsin mutants D85N, D85T, and D85,96N. *Biophys. J. 67*, 1682−1690.
(62) Song, L., El-Sayed, M. A., and Lanyi, J. K. (1993) Protein catalysis of the retinal subpicosecond photoisomerisation in the primary process of bacteriorhodopsin photosynthesis. *Science 261*, 891−894.
(63) Dobler, J., Zinth, W., Kaiser, W., and Oesterhelt, D. (1988) Excited-state reaction dynamics of bacteriorhodopsin studied by femtosecond spectroscopy. *Chem. Phys. Lett. 144*, 215−220.
(64) Du, M., and Fleming, G. R. (1993) Femtosecond time-resolved fluorescence spectroscopy of bacteriorhodopsin - direct observation of excited-state dynamics in the primary step of the proton pump cycle. *Biophys. Chem. 48*, 101−111.
(65) Schmidt, B., Sobotta, C., Heinz, B., Laimgruber, S., Braun, M., and Gilch, P. (2005) Excited-state dynamics of bacteriorhodopsin probed by broadband femtosecond fluorescence spectroscopy. *Biochim. Biophys. Acta 1706*, 165−173.
(66) Logunov, S. L., El-Sayed, M. A., and Lanyi, J. K. (1996) Catalysis of the retinal subpicosecond photoisomerization process in acid purple bacteriorhodopsin and some bacteriorhodopsin mutants by chloride ions. *Biophys. J. 71*, 1545−1553.
(67) Sharaabi, Y., Brumfeld, V., and Sheves, M. (2010) Binding of anions to proteorhodopsin affects the Asp97 pK_a. *Biochemistry 49*, 4457−4465.